Batteries & Supercaps

Research Article
doi.org/10.1002/batt.202500060

Chemistry Europe
European Chemical Societies Publishing

www.batteries-supercaps.org

Polyurethane/MXene Electrodes for Flexible Supercapacitor Applications

Jing Zhang, Yi Zhao, Jing Liu, Zhaoyang Li, Abdulraheem SA Almalki, Gaber A. M. Mersal, Mohamed M. Ibrahim, Hassan Algadi, Huige Wei,* Xuanye Wang, and Zhanhu Guo*

Conventional supercapacitors have encountered application bottlenecks due to their poor flexibility. In this context, a flexible polyurethane (PU)/MXene electrode is constructed by directly depositing MXene on PU substrate that is prepared by solvent casting method. In contrast to the pure MXene film, the elongation at break of the PU film prepared with a mass fraction of 9% reaches up to 435%, 94 times higher than that of the pure MXene film. At an optimum loading amount of 1.6 mg·cm^{-2}, PU/MXene film delivers a high mass-specific capacitance of 276 F·g^{-1}, 1.57 times that of 175 F·g^{-1} for pure MXene, at a current density of 1-A·g^{-1} under the three-electrode system. In the two-electrode system with polyvinyl alcohol/sulfuric acid as the gel electrolyte, the PU/MXene//PU/MXene-based symmetrical supercapacitor exhibits a high mass-specific capacitance of 123.2 F·g^{-1} at 0.5 A·g^{-1}, with a power density of 630.8-W·kg^{-1}, corresponding to an energy density of 4.8 Wh·kg^{-1}. The device still maintains 80.2% of the initial capacitance after 5000 cycles. In addition, there is no remarkable decrease in the electrochemical performance after repeated bending at different angles. This study provides a promising strategy for the facile preparation of high-performance flexible supercapacitors.

1. Introduction

With the increasing awareness of environmental protection[1,2] and shortage of fossil resources,[3] green sustainable energies such as batteries, solar cells, and fuel cells are in urgent need. In recent years, the demand for portable flexible wearable electronic devices has been growing.[4,5] However, for conventional energy storage devices such as lithium/sodium ion batteries,[6] the active electrode material is prone to separation from the collector when deformations such as bending and folding occur,[7] which leads to the failure of the energy storage device and sometimes, may even bring in safety issues, failing to meet the requirements of flexible electronics.[8] Therefore, it is imperative to develop energy storage devices with both reliable mechanical properties and excellent electrochemical performances to satisfy the practical applications.[9] Flexible supercapacitors (FSCs) have garnered extensive attention owing to their merits such as high power density and excellent stability.[10]

The electrode material is the core component that determines the performance of the FSCs.[11,12] Till now, new electrode materials have been explored, such as layered double hydroxide (LDH) materials,[13] metal-ogranic frameworks (MOFs), and their composite materials.[14–16] However, these two electrode materials have disadvantages such as low electrical conductivity and poor structural stability. MXene has proved to be an outstanding electrode material for applications in electrochemical energy storage devices.[17] However, the mechanical properties of pure MXene electrode are not satisfying. In order to fully utilize the excellent performance of MXene and further enhance the mechanical properties, MXene was often compounded with other polymers to obtain composite fibers.[18–20] In our previous work,[21] an interface-engineered strategy approach was proposed to prepare polylactic acid (PLA)/polyaniline (PANI)/MXene (PPM) film electrodes with high mechanical strength, excellent flexibility, and good electrochemical storage performance. Although PPM had some certain flexibility, the elongation at break was only 11.09%, which is sufficient for FSC applications.

In this context, polyurethane (PU) film was prepared by solvent volatilization method and used as the flexible substrate for MXene. PU films have advantages of high tensile strength and high temperature resistance, rendering them ideal as flexible

J. Zhang, Y. Zhao, J. Liu, Z. Li, H. Wei, X. Wang
Tianjin Key Laboratory of Brine Chemical Engineering and Resource Eco-utilization
College of Chemical Engineering and Materials Science
Tianjin University of Science and Technology
Tianjin 300457, China
E-mail: huigewei@tust.edu.cn

A. S. A. Almalki, G. A. M. Mersal, M. M. Ibrahim
Department of Chemistry
College of Science
Taif University
P.O. Box 11099, Taif 21944, Saudi Arabia

Z. Guo
Department of Mechanical and Construction Engineering
Northumbria University
Newcastle Upon Tyne NE1 8ST, UK
E-mail: zhanhu.guo@northumbria.ac.uk

H. Algadi
Department of electrical engineering
College of Engineering
Najran University
Najran 11001, Saudi Arabia

Supporting information for this article is available on the WWW under https://doi.org/10.1002/batt.202500060

Research Article
doi.org/10.1002/batt.202500060
Chemistry Europe
European Chemical Societies Publishing

substrates.[22] The experimental results show that when the mass fraction of PU is 9%, the mechanical properties are the best, and the elongation at break can reach 435% (94 times that of pure MXene film). PU/MXene flexible electrode films were prepared by loading MXene on 9% PU substrate by a facile "dip-coating–drying" method. The reason why MXene can be successfully loaded on PU films is that the amino and carboxyl groups of PU polymers form hydrogen bonds with the functional groups on the surface of MXene, forming dynamic interactions.[23,24] When the optimal mass load per unit area of MXene on PU is 1.6 mg·cm^{-2}, the prepared PU/MXene-1.6 film electrode obtains a high mass-specific capacitance of 275.9 F·g^{-1} at 1 A·g^{-1} in the three-electrode setup. It is ≈1.4 times that of pure MXene 190.8 F·g^{-1}. The symmetric solid-state supercapacitor of PU/MXene-1.6-SC based on PU/MXene-1.6 can obtain a high mass-specific capacitance of 123.2 F·g^{-1} at the current density of 0.5 A·g^{-1}, and the corresponding power density is 630.8 W·kg^{-1} and the energy density is 4.8 Wh·kg^{-1}. At 3 A·g^{-1}, the PU/ MXene-1.6-SC can still maintain an initial capacitance of 80.2% after 5000 cycles. In addition, after repeated bending experiments at different angles, there is no significant decrease in the electrochemical performance of the device. This study provides a promising strategy for the preparation of high performance stretchable supercapacitors.

2. Results and Discussion

2.1. Preparation of PU/MXene Electrode and Structures

PU/MXene electrodes were prepared by via a repeated "dip-coating–drying" method, and the preparation process is shown in **Figure 1**. PU/MXene electrodes were obtained by hydrogen bonds formed between amino and carboxyl groups of PU polymers and the functional groups on the surface of MXene. The mass loading of MXene on PU can be easily controlled by varying the dip-coating times. In order to investigate the MXene loading on the electrochemical performance of PU/MXene electrodes, a series of PU/MXene electrodes labeled as PU/MXene-0.8, PU/MXene-1.3, PU/MXene-1.6, PU/MXene-2.2, PU/MXene-3.6, and PU/MXene-5.8 were prepared, where the last number indicates that the mass loading per unit area of MXene on PU is 0.8, 1.3, 1.6, 2.2, 3.6, and 5.8 mg·cm^{-2}, respectively.

As shown in **Figure 2**, the interaction between PU and MXene was further confirmed by the change in the contact angle. The contact angle of PU film with water is 73.6°, as shown in Figure 2a. The contact angle value for PU/MXene-1.6 film is 21.9°, as shown in Figure 2b. The reduction of water contact angle is caused by the hydrophilic functional groups on the surface of MXene.[25,26] The contact angle was also tested in 1 M H_2SO_4 electrolyte, and the values for PU and PU/MXene-1.6 are 77.4° and 55.4°, respectively, as shown in Figure 2c,d. The contact angle is less than 90°, indicating that there is an effective wettability between the electrode and the electrolyte, which is conducive to the rapid diffusion of electrolyte ions to the electrode/electrolyte interface.[27,28]

The microstructure of PU film and PU/MXene-1.6 film electrodes was observed by scanning electron microscope (SEM). PU film presents an almost smooth surface morphology, as shown in **Figure 3**a. Figure 3b is the SEM image of PU/MXene-1.6 film

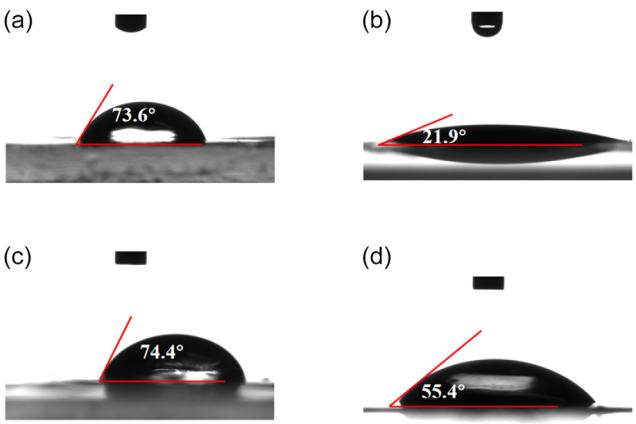

Figure 2. Contact angles of PU, PU/MXene films with a,b) deionized water and c,d) 1 M H_2SO_4 electrolyte.

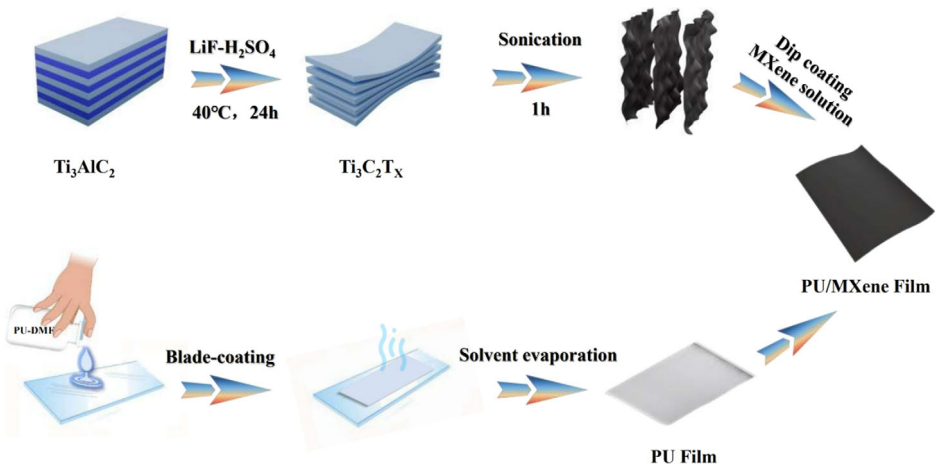

Figure 1. Preparation process of PU/MXene electrode.

Research Article
doi.org/10.1002/batt.202500060
Chemistry Europe
European Chemical Societies Publishing

electrode. The fold surface morphology of typical MXene nanosheets[29,30] can be seen, which proves that MXene successfully adheres to the PU surface. When the mass loading of MXene increases to 3.6 mg·cm^{-2}, serious accumulation can be observed and TiO_2 particles appear, which is the result of the oxidation of the surface of MXene.[31,32] This phenomenon is not good for the transfer of charge and would lead to the deterioration of the electrochemical performance.[33] Figure 3c,d shows the cross-sectional SEM images of PU and PU/MXene-1.6, from which it can be seen that MXene nanosheets with a certain thickness successfully adhere to the surface of the PU film.

The characteristic functional groups of PU and PU/MXene-1.6 films were verified by fourier transform infrared (FTIR) spectra (**Figure 4**a). In the PU film, the peaks at 3330, 2915, 1702, and 1732 cm^{-1} correspond to the carbamate group of PU.[34] In addition, the peak at 910 cm^{-1} corresponds to the epoxy group, the

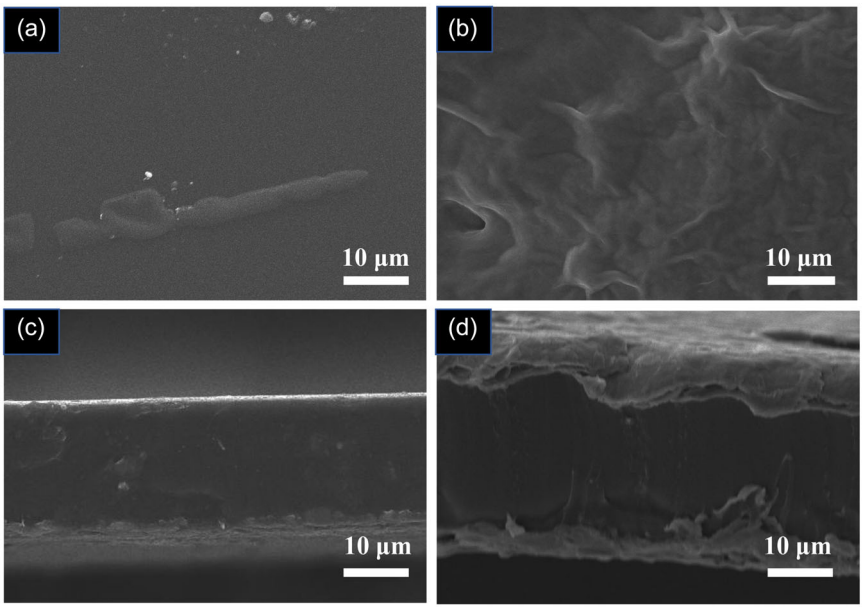

Figure 3. Top-view SEM images of a) PU and b) PU/MXene-1.6. Cross-sectional SEM images of c) PU and d) PU/MXene-1.6.

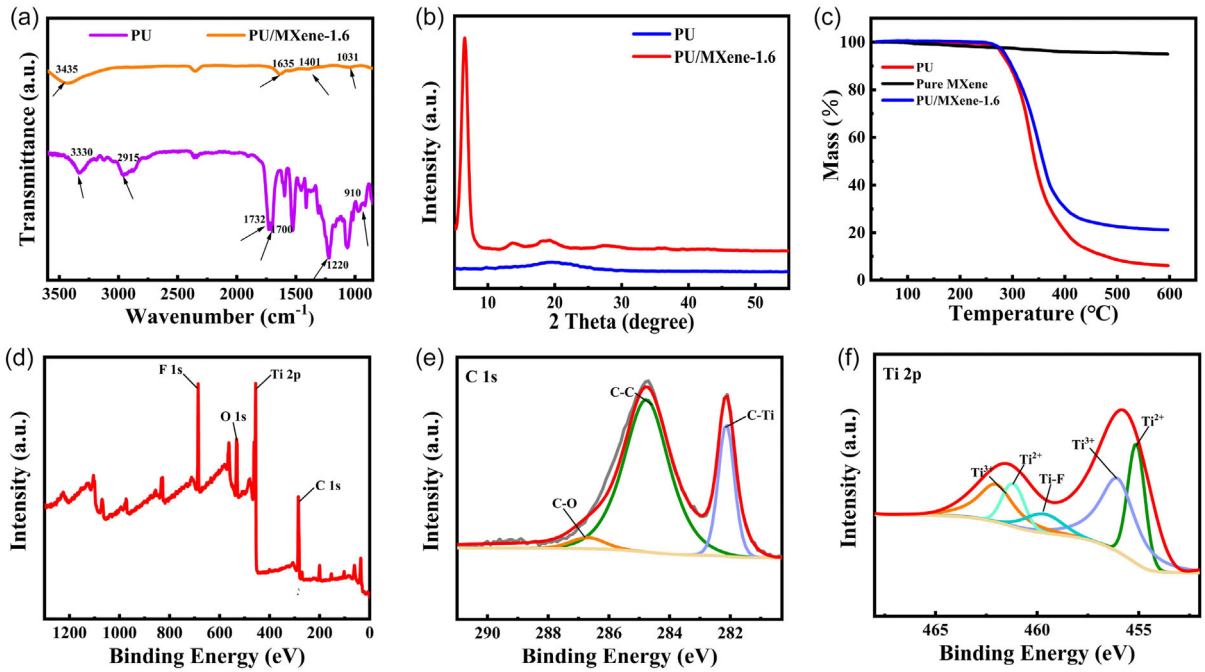

Figure 4. a) FTIR spectra of PU and PU/MXene-1.6. b) XRD patterns of PU and PU/MXene-1.6. c) TGA curves of PU, pure MXene, and PU/MXene-1.6. d) XPS survey spectra of PU/MXene-1.6. High-resolution spectra of e) C 1*s* and f) Ti 2*p* for PU/MXene-1.6.

Research Article
doi.org/10.1002/batt.202500060
Chemistry Europe
European Chemical Societies Publishing

peak at 1220 cm^{-1} shows the stretching vibration peak of C—O bond in ester, and the peaks of 1450-1650 cm^{-1} are attributed to the stretching vibration of benzene ring skeleton in PU hard segment structure. For PU/MXene-1.6 film electrode, the stretching vibration peaks at 3435, 1635, 1401, and 1031 cm^{-1} correspond to the characteristic functional groups —OH, C—O, O—H, and C—F for MXene.[35] Meanwhile, the characteristic peaks of PU are significantly weakened, which indicates that MXene is completely deposited on PU film.

Figure 4b demonstrates X-ray diffraction (XRD) patterns of PU and PU/MXene-1.6. PU film has a large and wide diffraction peak (001) at $2\theta = 20°$, which is characteristic of amorphous material materials. PU/MXene-1.6 film has a sharp peak (002) near $2\theta = 7°$, indicating a well-arranged layered structure of MXene.[36] The thermal stability of PU and PU/MXene-1.6 films is shown by thermogravimetric analysis (TGA) curves in Figure 4c. The weight percentage losses of pure MXene and PU film are 5.1% and 93.9%, respectively, at 600 °C, and the value for PU/MXene-1.6 film is 79.1%, which further confirms the deposition of MXene on PU film.

In order to study the bond configuration and elemental composition of PU/MXene-1.6, X-ray photoelectron spectroscopy (XPS) was performed. XPS displays the presence of C 1*s* and Ti 2*p* in PU/MXene-1.6 (Figure 4d). Figure 4e shows that the C 1*s* spectra of PU/MXene-1.6 can be fitted to three component peaks at 282.1, 284.8, and 286.7 eV, which belong to C—Ti, C—C, and C—O bonds, respectively.[37] The Ti 2*p* spectra of PU/MXene-1.6 (Figure 4f) can be fitted to three peaks of 455.1 eV (461.2 eV), 456.1 eV (462.1 eV), and 459.6 eV, corresponding to Ti^{2+}, Ti^{3+}, and Ti—F.[21] The presence of Ti^{2+}, Ti^{3+}, Ti—F, and C—Ti bonds indicates that MXene has successfully deposited on PU/MXene-1.6,[38] and the structure of MXene nanosheets is well preserved.

2.2. Mechanical Properties of Flexible Substrates

For wearable electronic devices to maintain long-term stability, safety, and reliable operation, excellent flexibility and stretchability are essential prerequisites to adapt to deformation conditions of bending, twisting, and stretching during use. **Figure 5**a shows the stress–strain curves of PU films with different mass fractions. When the mass fraction of PU film is 9%, the mechanical strength of PU film is the highest, with a tensile strength of up to 43.3 MPa and an elongation at break of up to 435%. Figure 5b shows the corresponding toughness of PU films with different mass fractions calculated from the stress–strain curves in Figure 5a. The results show that 9% PU film has a highest toughness of 85.8 $MJ{\cdot}m^{-3}$. Therefore, PU film with a mass fraction of 9% has the best mechanical properties and can be used as a flexible substrate.[39]

2.3. Electrochemical Performance

2.3.1. Three-Electrode System

In order to study the electrochemical performance of the prepared electrode, PU/MXene was used as the working electrode, platinum wire as the counter electrode, Hg/Hg_2SO_4 electrode as the reference electrode, and 1 M H_2SO_4 solution as the electrolyte. Measurements including cyclic voltammetry (CV), galvanostatic charge–discharge (GCD), and electrochemical impedance spectroscopy (EIS) were carried out. The charge transfer mechanism in PU/MXene electrodes is that the hydrogen ions in the electrolyte interact with the surface functional groups of MXene, thus causing the following surface oxidation reaction:[40]

$$Ti_3C_2O_x(OH)_yF_z + \delta e^- + \delta H^+ \leftrightarrow Ti_3C_2O_{x-\delta}(OH)_{y+}\delta F_z$$

Figure 6a shows the CV curves of PU/MXene with different MXene mass loadings at a scanning rate of 10 $mV{\cdot}s^{-1}$ and a voltage window of −0.7 to −0.1 V. It can be observed that with the increase of MXene mass loading per unit area, the enclosed area of PU/MXene electrode first increases and then decreases. When MXene mass loading is 1.6 $mg{\cdot}cm^{-2}$, the CV area reaches the maximum. The reason is that serious accumulation occurs when the loading of MXene is too high, as confirmed by Figure S1, Supporting Information. In the GCD curve, at the same current density (1 $A{\cdot}g^{-1}$), the discharge time of PU/MXene-1.6 is the longest (Figure 6b), which is consistent with the CV results, indicating that PU/MXene-1.6 has the best electrochemical performance.

Figure 6c shows the CV curves of the PU/MXene-1.6 at different scanning rates. As the scanning rate increases, the specific capacitance of PU/MXene-1.6 decreases because the electrolyte ions have less time to diffuse into the electrode material.[41] When

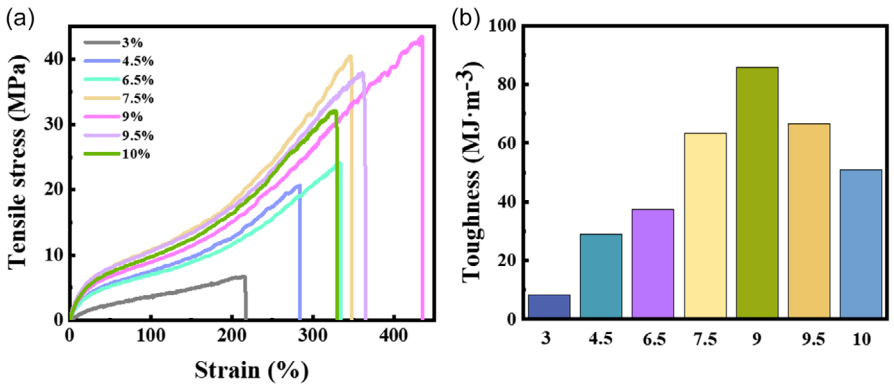

Figure 5. Mechanical properties of PU films: a) stress–strain curves of PU films with different mass fractions and b) the corresponding toughness.

Research Article
doi.org/10.1002/batt.202500060
Chemistry Europe
European Chemical Societies Publishing

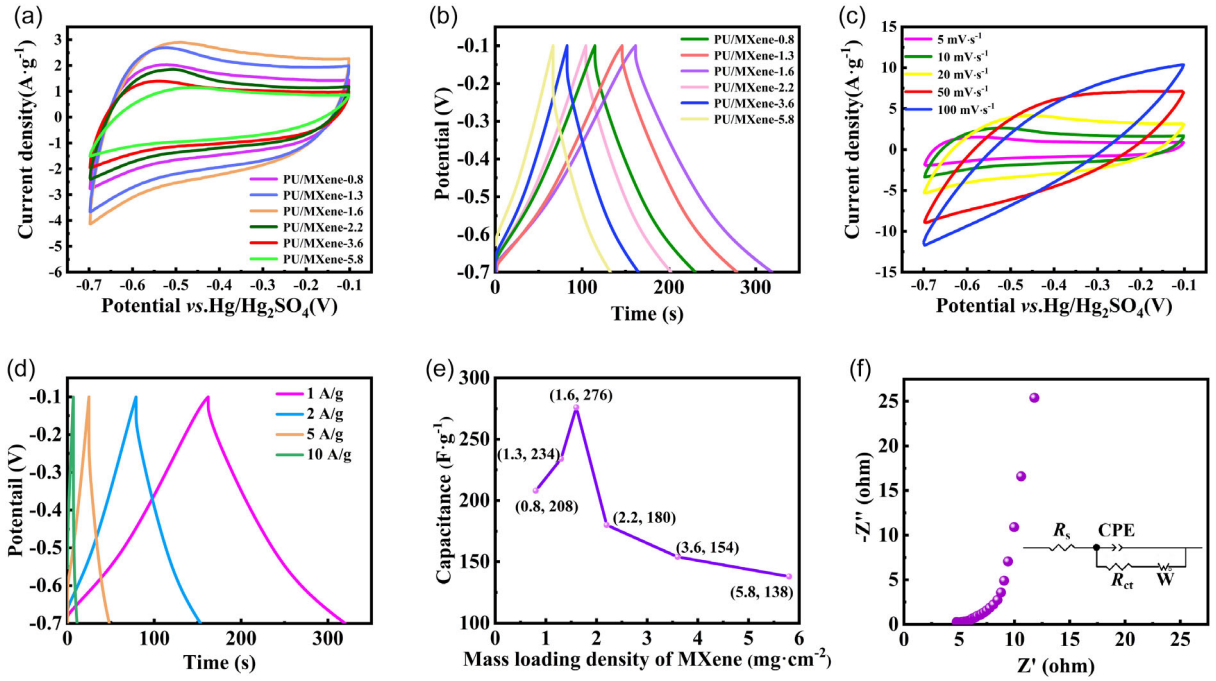

Figure 6. Electrochemical performance test of the PU/MXene-1.6 electrode. a) CV curves at a scan rate of 10 mV·s^{-1} for PU/MXene with different mass loadings of MXene. b) GCD curves at a current density of 1 A·g^{-1} for PU/MXene with different mass loadings of MXene. c) CV curves at different scan rates for PU/MXene-1.6. d) GCD curves at different current densities (1, 2, 5, 10 A·g^{-1}) for PU/MXene-1.6. e) Mass-specific capacitances of PU/MXene film electrodes with different mass loadings of MXene at a current density of 1 A·g^{-1}. f) Nyquist plot of PU/MXene-1.6.

the scanning rate is increased to 100 mV·s^{-1}, a small deformation of the CV curve can be observed, which may be caused by internal resistance in the electrode material. Figure 6d shows the GCD curves of the PU/MXene-1.6 electrode at different current densities (from 1 to 10 A·g^{-1}). All the curves exhibit good symmetry, indicating that the prepared electrode has a high Coulombic efficiency (CE). According to Equation S (5), Supporting Information, the CE of the PU/MXene-1.6 electrode at current densities of 1, 2, 5, and 10 A·g^{-1} is 97.24%, 94.08%, 93.88%, and 62.46%, respectively. At a low current density, the PU/MXene-1.6 electrode has a high *CE*. However, when the current density increases to 10 A·g^{-1}, the CE decreases. This may be because at a high current density, the rate of the electrode reaction accelerates. This leads to a faster consumption rate of reactants on the electrode surface, while the diffusion rate of reactants from the bulk solution to the electrode surface is relatively slow, thus causing concentration polarization.[42] The aggravation of the polarization phenomenon is expected to reduce the reversibility of the electrode reaction, and a part of the electrical energy would be consumed by side reactions or thermal energy caused by the insulating PU substrate, leading to a decrease in the CE.[43] Figure 6e shows the relationship between the mass specific capacitance values of PU/MXene electrodes and the mass load per unit area of MXene. The maximum capacitance of PU/MXene-1.6 electrode can reach 275.9 F·g^{-1}, 1.4 times that of the pure MXene electrode (190.8 F·g^{-1}). Figure S2, Supporting Information, shows the GCD curves of PU/MXene-1.6 film electrode and pure MXene electrode at current density 1 A·g^{-1}. It is clear that at a current density of 1 A·g^{-1}, the discharge time of the PU/MXene-1.6 electrode is significantly longer than that of the pure MXene film electrode. The reason is that the unique 2D layered structure of MXene is fully utilized using PU as the substrate while in pure MXene film electrode the nanosheets are stacked.

EIS measurements were performed at an open circuit voltage of 10 mV in the frequency range from 1 mHz to 100 kHz, as shown in Figure 6f. The Nyquist curve consists of a low-frequency line region and a high-frequency arc region. The intercept on the *Z'* real axis in the high-frequency region represents the internal resistance (R_s), and the semicircular diameter in the arc region represents the charge transfer resistance (R_{ct}).[44] In the low-frequency region in the three-electrode system, a line that is almost parallel to the *Y*-axis can be observed, suggesting that the prepared electrode has ideal capacitive characteristics.[21] No obvious semicircle is found in the high-frequency region, which indicates that the prepared electrode has a relatively small R_{ct}, which can be proved by the very small fitting values of 0.38 Ω from the equivalent circuit model, the inset of Figure 6f. The fitting values of R_s is 4.76 Ω. EIS results show that PU/MXene-1.6 film electrode exhibits excellent electrical conductivity, fast charge transfer, and diffusion rate.

2.3.2. Two-Electrode System

In order to explore the practical application of PU/MXene-1.6, a symmetric PU/MXene-1.6//PU/MXene-1.6 (PU/MXene-1.6-SC) solid flexible device was assembled using PVA/H_2SO_4 gel as the electrolyte and encapsulated by PDMS, as schematically shown in **Figure 7**a. Figure 7b shows CV curves of PU/MXene-1.6-SC devices with a voltage window ranging from 0 to 0.6 V and different

Research Article
doi.org/10.1002/batt.202500060
Chemistry Europe
European Chemical Societies Publishing

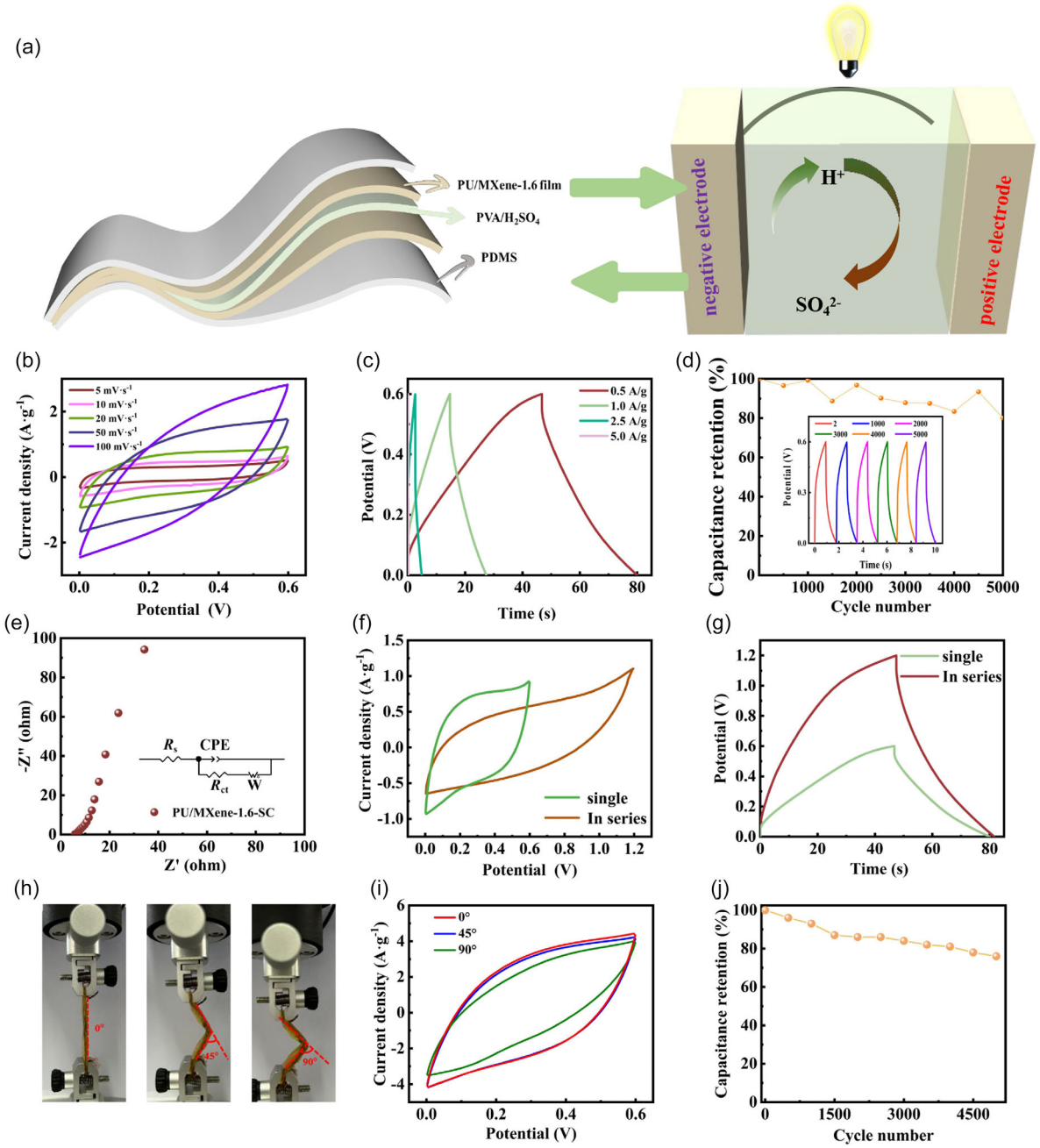

Figure 7. Electrochemical performance and flexibility tests of the PU/MXene-1.6-SC. a) Assembly diagram of two electrodes and encapsulation by PDMS. b) CV curves and c) GCD curves of PU/MXene-1.6-SC device at different scan rates and current densities, respectively. d) The cycling stability of the PU/MXene-1.6-SC device at a current density of 3 $A{\cdot}g^{-1}$, with the inset showing GCD curves recorded in the cycling testing. e) Nyquist plot of PU/MXene-1.6-SC. f) CV curves of two PU/MXene-1.6-SCs device connected in series (@ 20 $mV{\cdot}s^{-1}$) and g) GCD curves of two PU/MXene-1.6-SCs device connected in series (@ 0.5 $A{\cdot}g^{-1}$). h) Digital photographs showing PU/MXene-1.6-SC bent at different angles and i) the corresponding CV curves of PU/MXene-1.6-SC at a scan rate of 50 $mV{\cdot}s^{-1}$. j) The capacitance retention of PU/MXene-1.6-SC bent at 45° during 5000 charges/discharges cycles at a current density of 3 $A{\cdot}g^{-1}$.

scanning rates. Even at a high sweep speed of 100 $mV{\cdot}s^{-1}$, the CV curve shape changes very little, which represents an effective and rapid charge transfer, fully indicating that the electrode has an excellent ability to store charge.[45] In Figure 7c, the charge–discharge curve approximates as an isosceles triangle and a small voltage drop further reveals that the prepared flexible devices have excellent reversibility and good capacitance characteristics.[46,47] When the current density is 0.5 $A{\cdot}g^{-1}$, the mass specific capacitance reaches 123.2 $F{\cdot}g^{-1}$, and the corresponding power density and energy density are 630.8 $W{\cdot}kg^{-1}$ and 4.8 $Wh{\cdot}kg^{-1}$, respectively. In addition, according to Equation S (5), Supporting Information, the PU/MXene-1.6-SC has a relatively high CE of 71.21% at a current density of 0.5 $A{\cdot}g^{-1}$. Figure 7d shows the cyclic stability of the device. At 3 $A{\cdot}g^{-1}$, the PU/MXene-1.6-SC device can still maintain an initial capacitance of 80.2% after 5000 cycles, indicating an excellent cyclic stability. Figure 7e shows the Nyquist curve of the PU/MXene-1.6-SC device. The low frequency line area shows a vertical line almost parallel to the *Y*-axis, indicating that the

device has a relatively ideal capacitance.[21,48] The EIS results were fitted using the equivalent circuit model as shown in the inset of Figure 7e. The fitting values of R_s and R_{ct} are 5.76 Ω and 3.76 Ω, respectively. In addition, an EIS test was also conducted on the PU/MXene-1.6-SC after 5000 long-term cycling test, and the spectra were compared with that before the long-term cycle test (Figure S3, Supporting Information). After the long-term cycling, the R_s of PU/MXene-1.6-SC changes from 5.76 to 22.33 Ω, and the R_{ct} changes from 3.76 to 6.04 Ω, which may be caused by the deterioration of the gel electrolyte or reduced adhesion of MXene on PU substrate during the long-term cycling.[49,50]

In order to meet the requirement of high voltage in practical application, the prepared PU/MXene-1.6-SC was assembled in series. CV and GCD results show (Figure 7f–g) that the voltage window of the two devices in series extends from 0.6 to 1.2 V with consistency, indicating that the device is reliable for practical applications. In addition, the flexibility of PU/MXene-1.6-SC was evaluated. Figure 7h illustrates the definitions of different bending angles, and Figure 7i shows the corresponding CV curves of PU/MXene-1.6-SC after repeated bending. There was no remarkable decrease in the electrochemical performance when PU/MXene-1.6-SC is subject to bending. Figure 7j shows the capacitance retention of PU/MXene-1.6-SC during 5000 charge–discharge cycles at a current density of 3 $A{\cdot}g^{-1}$ bent at an angle of 45°. The result indicates that the capacitance retention rate is higher than 76% after 5000 cycles, indicating the promising prospect of PU/MXene-1.6-SC for applications in the field of flexible wearable electronic devices.

3. Conclusions

PU/MXene electrodes have been successfully prepared by loading MXene on PU film as a flexible substrate through repeated "dip-coating–drying" method. When the mass fraction of PU is 9%, the mechanical properties of PU film are the best, and the elongation at break can reach 435% (94 times that of pure MXene film). When the mass load of MXene on PU is 1.6 $mg{\cdot}cm^{-2}$, the prepared PU/MXene-1.6 thin film electrode obtains a high specific capacitance of 275.9 $F{\cdot}g^{-1}$ at 1 $A{\cdot}g^{-1}$ under the three-electrode setup. It is ≈1.4 times of pure MXene which is 190.8 $F{\cdot}g^{-1}$. The assembled symmetric solid-state supercapacitor based on PU/MXene-1.6 can obtain a high specific capacitance of 123.2 $F{\cdot}g^{-1}$ at a current density of 0.5 $A{\cdot}g^{-1}$, and the corresponding power density is 630.8 $W{\cdot}kg^{-1}$ and the energy density is 4.8 $Wh{\cdot}kg^{-1}$. At 3 $A{\cdot}g^{-1}$, the device can still maintain 80.2% of the initial capacitance after 5000 cycles. In addition, after repeated bending experiments at different angles, there is no significant change in the electrochemical performance. This study provides a facile strategy for large-scale preparation of high-performance FSCs.

4. Experimental Section

Materials

The materials used in this experiment were analytically pure except PU which was the standard grade. Titanium aluminum carbide (Ti_3AlC_2, 400 mesh) was purchased from 11 Technology Co., Ltd. (China). Anhydrous ethanol (99.7%) and H_2SO_4 (98 wt%) were supplied by Fengchuan Chemical (Tianjin, China). Lithium fluoride (LiF, $M_w = 25.94$, 99.9% metals basis) and polyvinyl alcohol (PVA, 95.5% hydrolyzed) were provided by Shanghai Aladdin Biochemical Technology Co., Ltd. Polydimethylsiloxane (PDMS) prepolymer and the curing agent were supplied by Shenzhen Ausbond Co., Ltd.

Preparation of PU/MXene Electrode

The prepared PU film was used as the substrate, washed with deionized water, and dried at room temperature. PU film was immersed in MXene suspension for 1 min and then dried in an oven at 50 °C for 0.5 h. The mass load of MXene on the PU film was controlled by varying the immersion times in the MXene suspension. Pure MXene membrane electrodes were prepared by vacuum filtration method as a control. For preparation of PU and MXene, please refer to Supporting Information.

Assembly of Symmetric Supercapacitors

A symmetrical supercapacitor (PU/MXene-1.6-SC) was constructed by sandwiching 1 M PVA/H_2SO_4 gel electrolyte between two identical PU/MXene-1.6 electrodes, and then encapsulated with two PDMS films and then protected by polyimide tape. For the preparation of PVA/H_2SO_4 gel electrolytes, please refer to Supporting Information.

Characterizations

The microstructure of the PU/MXene electrodes was analyzed by SEM on an Apreo of FEI Company (USA). The functional groups were characterized by Fourier infrared spectrometer of VECTOR-22 of Germany. The hydrophilicity of the electrode was tested by contact angle meter from Shanghai Jizhu Chemical Technology Co. Ltd. XRD patterns were collected by a Bruker D8 advanced diffractometer with Cu Kα radiation. XPS measurements were performed on Thermo Scientific Escalab 250Xi (USA). Thermogravimetric testing of PU, MXene, and PU/MXene-1.6 was performed with a NETZSCH STA449 F5 thermogravimetric analyzer (TGA). The mechanical properties were tested on a Uniaxial Materials Testing System (LIGAO, HF-9002) equipped with a 100 N load cell at room temperature.

Electrochemical Measurements

All electrochemical measurements were performed on an electrochemical workstation (ZAHNER, Germany). In the three-electrode system, the fabricated PU/MXene electrodes, a platinum wire, and Hg/Hg_2SO_4 electrode served as the working, counter, and reference electrode, respectively. The electrolyte was a 1 M H_2SO_4 solution. The voltage window for CV and GCD tests was −0.7 to −0.1 V. Scan rates for CV tests were 5, 10, 20, 50, and 100 $mV{\cdot}s^{-1}$. The current densities of GCD tests were 1, 2, 5, and 10 $A{\cdot}g^{-1}$. EIS was tested at frequencies from 10 mHz to 100 kHz with an amplitude of 10 mV. In the two-electrode system, all electrochemical measurements of symmetric all-solid supercapacitor were determined using 1 M H_2SO_4/PVA gel electrolyte. The voltage window for CV and GCD tests was 0 to −0.6 V. Scan rates for CV tests included 5, 10, 20, 50, and 100 $mV{\cdot}s^{-1}$. The current densities of GCD tests included 0.5, 1, 2.5, and 5 $A{\cdot}g^{-1}$. The values of capacitance, energy density, and power density were calculated according to the Equation S (1)–(4), Supporting Information.

Acknowledgements

J.Z. and Y.Z. contributed equally to this work. This research was supported by the National Training Program of Innovation and

Entrepreneurship for Undergraduates (grant no. 202410057256). The authors extend their appreciation to Taif University, Saudi Arabia for supporting this work through project number (TU-DSPP-2024-03).

Conflict of Interest

The authors declare no conflict of interest.

Data Availability Statement

The data that support the findings of this study are available from the corresponding author upon reasonable request.

Keywords: flexible supercapacitors · MXene · polyurethane

[1] A. Kinyar, K. Bothongo, *Energy* **2025**, *314*, 134117.
[2] A. Seilkhan, A. Kuatbayev, G. Satybaldiyeva, B. Akbota, S. Zhang, G. Xiaojiang, Z. Idrisheva, S. Issabayeva, *ES Energy Environ.* **2024**, *26*, 1338.
[3] S. Ahmed, M. S. Islam, U. B. Antu, M. M. Islam, V. D. Rajput, N. A. Mahiddin, J. R. Paul, Z. Ismail, K. A. Ibrahim, A. M. Idris, *Inter. J. Bio. Macromol* **2025**, *285*, 137979.
[4] Y. Myung, T. Kim, *Batter. Supercaps* **2024**, *7*, e202400557.
[5] A. Tandon, S. Rani, Y. Sharma, *Batter. Supercaps* **2024**, *7*, e202400176.
[6] S. Sirikasemsuk, P. Vengsungnle, S. E. Eiamsa-ard, P. Naphon, *Eng. Sci.* **2024**, *27*, 1017.
[7] X. M. Jiang, Y. J. Chen, X. K. Meng, W. G. Cao, C. C. Liu, Q. Huang, N. Naik, V. Murugadoss, M. A. Huang, Z. H. Guo, *Carbon* **2022**, *191*, 448.
[8] I. Aimbetova, A. Kuzmin, K. Sarbaeva, M. Sarbaeva, G. Satybaldiyeva, *ES Energy Environ.* **2024**, *26*, 1339.
[9] Z. Huang, Y. Peng, J. Zhao, S. Zhang, P. Qi, X. Qu, F. Yan, B. Ding, Y. Xuan, X. Zhang, *Nano-Micro Lett.* **2024**, *17*, 98.
[10] R. R. Palem, M. C. Devendrachari, I. Rabani, V. Nulu, N. S. Kumar, M. Asif, Y.-S. Seo, S.-H. Lee, *Int. J. Biol. Macromol.* **2024**, *278*, 134707.
[11] S. Kumar, G. Saeed, L. Zhu, K. N. Hui, N. H. Kim, J. H. Lee, *Chem. Eng. J.* **2021**, *403*, 126352.
[12] Y. Zhao, W. J. Qiao, H. Z. Wang, Y. Y. Xie, B. T. Teng, J. R. Li, Y. L. Sun, A. S. Alsubaie, T. Wan, S. M. El-Bahy, D. P. Cui, Z. M. El-Bahy, J. Zhang, H. G. Wei, Z. H. Guo, *Carbon* **2024**, *230*, 119665.
[13] L. Zhang, R. Chen, K. N. Hui, K. S. Hui, H. Lee, *Chem. Eng. J.* **2017**, *325*, 554.
[14] K. Wang, K. N. Hui, K. San Hui, S. Peng, Y. Xu, *Chem. Sci.* **2021**, *12*, 5737.
[15] J. Hou, Y. Ning, K. Guo, W. Jiao, C. Chen, B. Zhang, X. Wu, J. Zhao, D. Lin, S. Sun, *J. Energy Storage* **2025**, *113*, 115535.
[16] P. Duan, W. L. Dai, Z. X. Wang, M. Chen, L. Niu, T. Z. Wu, L. Zeng, G. Feng, *Batter. Supercaps* **2024**, *7*, e202300536.
[17] X. Wang, S. Kajiyama, H. Iinuma, E. Hosono, S. Oro, I. Moriguchi, M. Okubo, A. Yamada, *Nat. Commun.* **2015**, *6*, 6544.
[18] T. Yuan, Z. Zhang, Q. Liu, X.-T. Liu, S.-Q. Tao, C.-l. Yao, *Int. J. Biol. Macromol.* **2024**, *262*, 130119.
[19] P. Yang, Z. Li, D. Zhang, K. Yang, Y. Ling, T. Zhang, Q. Quan, C. Liu, W. Chen, X. Zhou, *Int. J. Biol. Macromol.* **2024**, *279*, 135476.
[20] W. Fan, Q. Wang, K. Rong, Y. Shi, W. Peng, H. Li, Z. Guo, B. B. Xu, H. Hou, H. Algadi, S. Ge, *Nano-Micro Lett.* **2023**, *16*, 36.
[21] Z. Li, J. Li, B. Wu, H. Wei, H. Guo, Z. M. El-Bahy, B. Liu, M. He, S. Melhi, X. Shi, *J. Mater. Sci. Technol.* **2024**, *203*, 201.
[22] H. Park, J. W. Kim, S. Y. Hong, G. Lee, H. Lee, C. Song, K. Keum, Y. R. Jeong, S. W. Jin, D. S. Kim, J. S. Ha, *ACS Nano* **2019**, *13*, 10469.
[23] J. Zhou, D. Shi, Y. Wang, M. Chen, W. Dong, *Mater. Res. Bull.* **2022**, *154*, 111939.
[24] I. T. Liu, P. Meemai, Y.-H. Lin, C.-J. Fang, C.-C. Huang, C.-Y. Li, M. Phisalaphong, J.-L. You, S.-H. Tung, R. Balaji, Y.-C. Liao, *Int. J. Biol. Macromol.* **2024**, *281*, 135804.
[25] A. Chen, H. Wei, Z. Peng, Y. Wang, S. Akinlabi, Z. Guo, F. Gao, S. Duan, X. He, C. Jia, *Small* **2024**, 2404011.
[26] T. Zhang, X. Guo, B. Solomon, M. Sharifpur, L.-Z. Zhang, *J. Membr. Sci.* **2022**, *644*, 120146.
[27] L. Zhao, Y. Y. Peng, P. Y. Dou, Y. Li, T. Q. He, F. Ran, *InfoMat* **2024**, e12597.
[28] D. H. Jeon, *Energy Storage Mater.* **2019**, *18*, 139.
[29] J. C. Lei, X. Zhang, Z. Zhou, *Front. Phys.* **2015**, *10*, 276.
[30] W. K. Xu, Z. A. Shi, Z. Y. Yu, C. Peng, G. X. Yang, H. F. Wang, J. N. Huang, Y. H. Cao, H. J. Wang, L. B. Li, H. Yu, *Nano Lett.* **2024**, 10547.
[31] R. A. Soomro, P. Zhang, B. M. Fan, Y. Wei, B. Xu, *Nano-Micro Lett.* **2023**, *15*, 108.
[32] F. Xia, J. Lao, R. Yu, X. Sang, J. Luo, Y. Li, J. Wu, *Nanoscale* **2019**, *11*, 23330.
[33] Z. W. Gao, W. R. Zheng, L. Y. S. Lee, *Small* **2019**, *15*, 1902649.
[34] H. Cheng, C. Yang, J. Chu, H. Zhou, C. Wang, *Sen. Actuat. A-Phys.* **2023**, *353*, 114226.
[35] T. Bai, W. G. Wang, G. F. Xue, S. Y. Li, W. X. Guo, M. D. Ye, C. X. Wu, *ACS Appl. Mater. Interfaces.* **2021**, *13*, 57576.
[36] Y. Yoon, M. Lee, S. K. Kim, G. Bae, W. Song, S. Myung, J. Lim, S. S. Lee, T. Zyung, K. S. An, *Adv. Energy Mater.* **2018**, *8*, 1703173.
[37] A. L. Chen, C. Y. Wang, O. A. A. Ali, S. F. Mahmoud, Y. T. Shi, Y. X. Ji, H. Algadi, S. M. El-Bahy, M. A. Huang, Z. H. Guo, D. P. Cui, H. G. Wei, *Compos. Pt. A-Appl. Sci. Manuf.* **2022**, *163*, 11.
[38] C. Liu, Y. Bai, W. Li, F. Yang, G. Zhang, H. Pang, *Angew. Chem. Int. Ed.* **2022**, *61*, e202116282.
[39] M. P. Sidheekha, A. Shabeeba, L. Rajan, M. S. Thayyil, Y. A. Ismail, *Eng. Sci.* **2023**, *23*, 890.
[40] M. R. Lukatskaya, S. Kota, Z. F. Lin, M. Q. Zhao, N. Shpigel, M. D. Levi, J. Halim, P. L. Taberna, M. Barsoum, P. Simon, Y. Gogotsi, *Nat. Energy* **2017**, *2*, 17105.
[41] J. Tang, T. Mathis, X. W. Zhong, X. Xiao, H. Wang, M. Anayee, F. Pan, B. M. Xu, Y. Gogotsi, *Adv. Energy Mater.* **2021**, *11*, 2003025.
[42] C. Bodin, C. S. Bongur, M. Deschanels, S. Catrouillet, S. Le Vot, F. Favier, O. Fontaine, *Batter. Supercaps* **2020**, *3*, 1193.
[43] K. C. Sowmiya, K. A. Vijayalakshmi, *Appl. Phys. A-Mater. Sci. Process.* **2024**, *130*, 583.
[44] S. Liu, K. S. Hui, K. N. Hui, H. F. Li, K. W. Ng, J. C. Xu, Z. K. Tang, S. C. Jun, *J. Mater. Chem. A* **2017**, *5*, 19046.
[45] S. Chanthee, C. Asavatesanupap, D. Sertphon, T. Nakkhong, N. Sub, jalearndee, M. Santikunaporn, *Eng. Sci.* **2023**, *27*, 975.
[46] G. Y. Yuan, T. Wan, A. BaQais, Y. R. Mu, D. P. Cui, M. A. Amin, X. D. Li, B. B. Xu, X. H. Zhu, H. Algadi, H. D. Li, P. Wasnik, N. Lu, Z. H. Guo, H. G. Wei, B. W. Cheng, *Carbon* **2023**, *212*, 118101.
[47] C. L. Li, S. Wang, X. R. Wang, W. Y. Bai, H. Sun, F. Pan, Y. Chi, Z. Wang, *ACS Mater. Lett.* **2023**, *5*, 2084.
[48] L. Y. Qing, J. Jiang, *ACS Nano* **2023**, *17*, 17122.
[49] Q. H. Wu, T. Q. He, Y. K. Zhang, J. L. Zhang, Z. J. Wang, Y. Liu, L. Zhao, Y. Z. Wu, F. Ran, *J. Mater. Chem. A* **2021**, *9*, 24094.
[50] S. Liu, Y. Yin, M. S. Wu, K. S. Hui, K. N. Hui, C. Y. Ouyang, S. C. Jun, *Small* **2019**, *15*, 1803984.

Manuscript received: January 27, 2025
Revised manuscript received: June 24, 2025
Version of record online: